CONFERENCE PRE-PRINT

Energetic-electron-driven Geodesic Acoustic Mode Interaction with Microtearing Mode for Improved Confinement on HL-3 Tokamak

[1]S.Q. Wang, [2]X.L. Zou, [1]X.R. Duan, [1]A.S. Liang, [1]L.M. Yu, [1]G.L. Xiao, [1]Y.R. Zhu, [1]M.K. Han, [1,3]Y. Zhou, [1]T.F. Sun, [1]A. Wang, [1]S.B. Gong, [1]W.P. Guo, [1]Q.L. Yang, [1]Y.G. Li, [1]H.X. Wang, [1]M. Jiang, [1]Y.P. Zhang, [1]D.L. Yu, [1]Z.B. Shi, [1]W. Chen, [1]W.L. Zhong and [1]HL-3 Team

[1]Southwestern Institute of Physics, Chengdu, People's Republic of China
[2]CEA, IRFM, Saint-Paul-Lez-Durance, France
[3]Department of Engineering Physics, Beijing, People's Republic of China

Email: wangshiqin@swip.ac.cn

Abstract

We report the first observation of microtearing mode (MTM) and its interaction with energetic-particle-induced geodesic acoustic mode (EGAM) in the reduction of ambient turbulence, leading to improvements in energy and particle confinements in electron cyclotron resonance heating (ECRH) plasma on HL-3 tokamak. MTM, observed in the magnetic fluctuation spectrum with a frequency range of 80-120 kHz, is found to be driven by the electron temperature gradient. It has been shown that MTM propagates in the electron diamagnetic drift direction with a poloidal normalized wavenumber $0.05 \leq k_\theta \rho_s \leq 0.17$. The $n=0, m=-2$ magnetic structure of EGAM with a frequency range of 14-20 kHz is observed in the magnetic fluctuation spectrum, where n and m are the toroidal and poloidal mode numbers, respectively. The $V_{E\times B}$ oscillation of EGAM has also been observed in the Doppler reflectometry phase derivative perturbation spectrum. The frequency of EGAM corresponds to half that of the conventional GAM. Bispectral analysis during ECRH shows pairwise interactions among EGAM, MTM and ambient turbulence (low frequency). It has been found that the reduction of ambient turbulence due to MTM and EGAM leads to the improvement of particle and energy confinements. Experimental results on HL-3 show the interaction between MTM and EGAM provides a possible way to the turbulence control for energy and particle confinement improvements in future reactors.

1. INTRODUCTION

Plasma transport is one of the critical issues in magnetic confinement fusion research. Researches in the past decades show that the plasma confinement is largely influenced by drift turbulence and associated turbulence transport [1].

MTM is an electromagnetic microinstability [2], driven by electron temperature gradient and propagates in the electron diamagnetic drift direction. MTM is an ion scale mode, with $k_\theta \rho_s < 1$ [2]. MTMs have been observed in an edge transport barrier (ETB) on tokamak [3], and in an internal transport barrier (ITB) on reversed field pinch (RFP) device [4]. The RFP device provides direct observation of small-scale MTMs and their amplitudes are correlated to the electron temperature gradient in the plasma core [4]. The experimental, theoretical and simulation results have shown that MTM has strong effects on electron thermal transport [5] and little impact on particle transport [3].

Geodesic acoustic modes (GAMs) can be driven by energetic particle, called energetic-particle-driven geodesic acoustic modes (EGAMs) [6]. EGAMs have a significant magnetic component, and usually exist

closely to the plasma core region [7] unlike the turbulence-driven GAMs which tend to be excited near the edge region [8] in tokamaks. EGAM is a global mode with a finite radial spatial extent, which can extend to a few tens of precent of the plasma minor radius [6]. In contrast, the conventional GAM typically has a much smaller radial width, generally translating to a width range of 1-5 cm [6]. The EGAM frequencies are significantly lower than the conventional GAM frequencies by a factor of approximately 2 [9,10].

Nonlinear interactions usually have two kinds of processes including modulation and synchronization, which can change the plasma transport and confinement. Previous experimental results show the existence of interaction between GAM and ambient turbulence in JET [11]. Gyrokinetic simulations results using the GYSELA code showed a complex interaction between EGAMs and ITG turbulence, leading to a radial propagation of ITG turbulence thus unable to suppress the ITG turbulence [12]. The relations between MTM and EGAM, MTM and ambient turbulence, and the influence on transport are not yet clear.

The paper is organized as follows. In section 2, the experimental setup and the key diagnostics are introduced. Section 3 presents the characterization of EGAM and the identification of MTM. Section 4 mainly analyzes the interaction among MTM, EGAM and ambient turbulence (low frequency turbulence). In addition, section 4 shows the effects of MTM, EGAM and ambient turbulence on energy and particle confinements. Finally, conclusions and discussions are presented in section 5.

2. EXPERIMENTAL SETUP

HL-3 is a new medium-sized tokamak at Southwestern Institute of Physics (SWIP), dedicated to conducting advanced operation scenarios and frontier physics research related to burning plasma [13]. The major radius and minor radius are R=1.78 m and a=0.65 m, respectively. In discharge #4742, the plasma current is I_p~300 kA and the toroidal magnetic field B_t=1.51 T. A two-period ECRH is applied in the auxiliary heating system, changing from 0.34 MW to 0.42 MW.

The plasma line averaged electron density is obtained by far-infrared laser interferometer (FIR). Radial profiles of the electron density n_e and temperature T_e are measured with Thomson Laser scattering (TS). The Mirnov coils consist of poloidal arrays (41 probes covering both low-field side and high-field side) and two sets of toroidal arrays, with 12 probes in low-field side (LFS) and 12 probes in high-field side (HFS). On HL-3 tokamak, the Doppler Reflectometer (DR) has been developed to measure the perpendicular rotation velocity of plasma turbulence.

3. OBSERVATION OF EGAM AND MTM

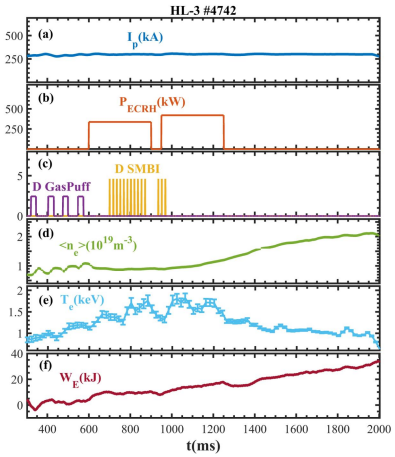

Fig. 1. Time traces of discharge #4742 on HL-3 tokamak showing the (a) plasma current, (b) ECRH power, (c) gas puffing and SMBI pulses of deuterium, (d) line-averaged electron density, (e) core electron temperature and (f) plasma stored energy.

Figure 1 presents the time traces of discharge #4742 with ECRH on HL-3 tokamak. The plasma current is 300 kA as shown in figure 1(a). Figure 1(b) displays the ECRH power with two periods of injection and the heating powers are 0.34 MW and 0.42 MW, respectively. Figure 1(c) shows the gas puffing pulses (purple) and the SMBI pulses (orange) of deuterium. Figure 1(d) is the line-averaged electron density. The density was changed due to gas puffing before ECRH power injection, almost unchanged after ECRH injection with SMBI pulses, and increases after second ECRH injection. The core electron temperature and stored energy also gradually increase after ECRH input as shown in figure 1(e) and figure 1(f).

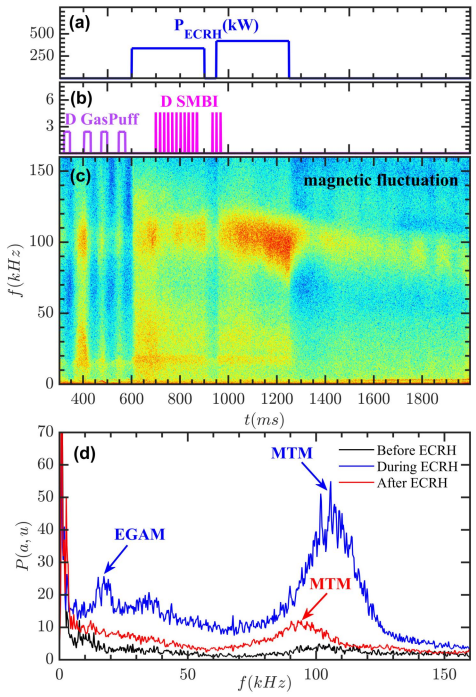

Fig. 2. (a) ECRH power, (b) gas puffing and SMBI pulses of deuterium, (c) magnetic fluctuation spectrum of poloidal Mirnov coil , (d) power spectra of the magnetic fluctuations before ECRH at t=340-350 ms, during ECRH at t=1000-1050ms, and after ECRH at t=1600-1650ms.

Figure 2(c) shows the magnetic fluctuation spectrum measured by the poloidal Mirnov probe (‘MDBP01’) in the HFS. From the power spectrum of the magnetic fluctuations during ECRH in figure 2(d), it can be observed that there is a quasi-coherent mode (QCM) with a frequency range of 14-20 kHz and a broadband fluctuation with a frequency range of 80-120 kHz. The broadband magnetic fluctuations, which are electromagnetic turbulence, will be analyzed later in detail and identified as MTM. The QCM with a frequency range of 14-20 kHz will be identified as EGAM.

3.1 Characterization of EGAM

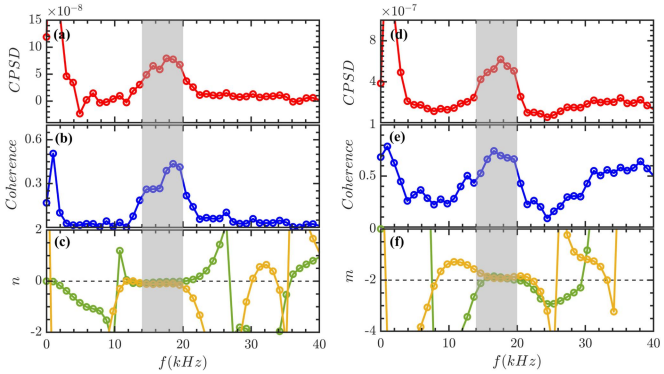

Fig. 3. (a) Cross power spectral density and (b) coherence coefficient of toroidal Mirnov signals and (c) toroidal mode numbers, (d) cross power spectral density and (e) coherence coefficient of poloidal Mirnov signals and (f) poloidal mode numbers.

The QCM with a frequency range of 14-20 kHz is observed in the magnetic fluctuation spectrum as shown in figures 2(c) and 2(d). It is obvious that the toroidal mode number and the poloidal mode number of the QCMs with the frequency range of 14-20 kHz in the shaded region of figures 3(c) and 3(f) is $n = 0$ and $m = -2$. Both theory and experiment results indicate that the magnetic component of GAM is given by an n=0, m=±2 structure that can be measured externally [6], thus the QCM of 14-20 kHz observed in magnetic fluctuation spectrum has the same magnetic structure as GAM.

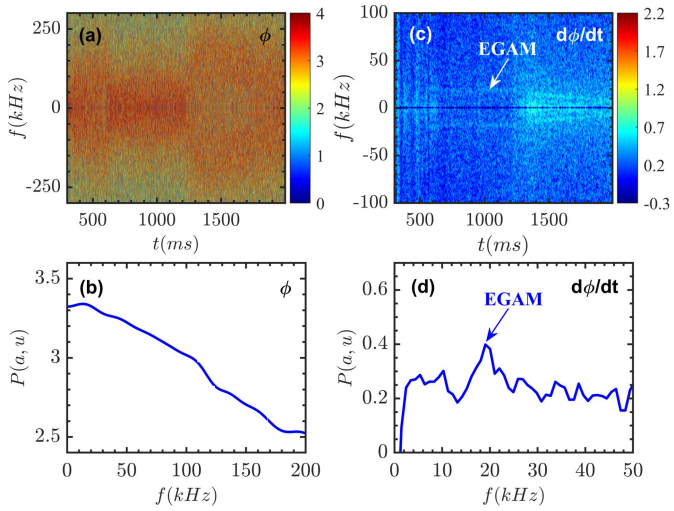

Fig. 4. (a) Phase fluctuation spectrogram of DR (52.5 GHz) at ρ≈0.45, (b) power spectrum of the phase fluctuation during ECRH at t=1000-1010 ms, (c) spectrogram of DR phase derivative perturbation $(d\tilde{\phi}/dt)$ at 52.5 GHz around ρ≈0.45 and (d) power spectrum of the DR phase derivative perturbation during ECRH at t=1000-1100 ms.

The QCM of 14-20 kHz is observed in the DR phase derivative perturbation, but not seen in the phase fluctuation as shown in figure 4, these indicate the QCM of 14-20 kHz represents the $E\times B$ velocity oscillation $(\tilde{V}_{E\times B})$. The coherence coefficient of $V_{E\times B}$ fluctuation and the magnetic fluctuation indicate the QCMs of 14-20 kHz in $V_{E\times B}$ and magnetic fluctuation power spectrum are the same modes.

The finite-frequency zonal flow, known as the geodesic acoustic mode (GAM), exhibit such characteristics. The frequency formula of conventional GAM is based on the Winsor's fluid model $f_{GAM}= C_s\sqrt{2+1/q^2}/(2\pi R_0)$ [6], where $C_s=\sqrt{(T_e+T_i)/m_i}$ is the ion sound velocity. Based on this formula, the predicted frequency of

conventional GAM is f_{GAM}~34.7 kHz, here $T_i \approx T_e \approx 700$ eV and q~2, which is very close to twice the frequency corresponding to the QCM maximum value of about 17 kHz. The frequency of this QCM is consistent with that of the EGAM. The QCMs of 14-20 kHz are observed in two channels of the $V_{E\times B}$ fluctuation at 52.5 GHz and 55 GHz around $\rho \approx 0.45$ and $\rho \approx 0.42$, respectively. All of these observations indicate that the QCM of 14-20 kHz suggests EGAM.

3.2 Identification of MTM

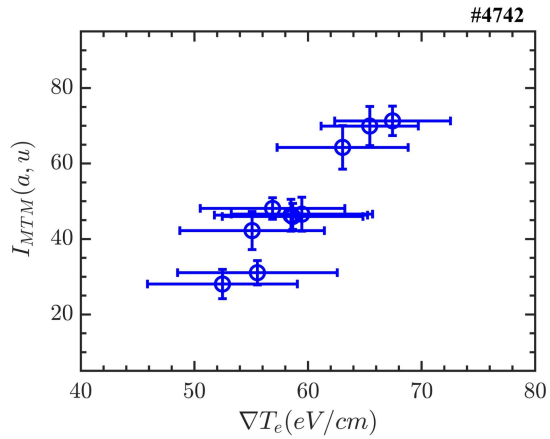

Fig. 5. Intensity of the electromagnetic turbulence vs electron temperature gradient.

The relationship between the intensity of the electromagnetic turbulence of 80-120 kHz and the electron temperature gradient is shown in figure 5. It is shown that there is a strong correlation between the intensity of this electromagnetic turbulence within the 80-120 kHz frequency range and electron temperature gradient at ρ=0.2, indicating that this turbulence is driven by the electron temperature gradient.

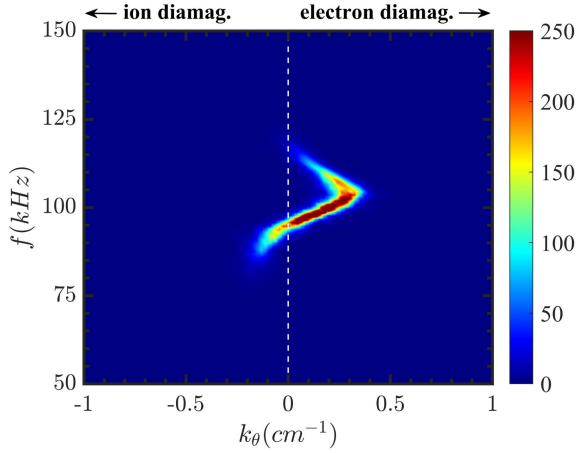

Fig. 6. Poloidal wave-spectrum of the magnetic fluctuations with a filtering frequency range of 50-150 kHz from 'MDBP02' and 'MDBP03'.

The poloidal array of Mirnov coils can be used for correlation analysis in poloidal directions. The figure 6 shows the poloidal wave-number spectrogram $S(k_\theta, f)$ obtained from the two poloidal Mirnov coils. It can be indicated that the high frequency electromagnetic turbulence of 80-120 kHz has a poloidal normalized wavenumber $0.05 \leq k_\theta \rho_s \leq 0.17$, here $\rho_s = C_s/\Omega_i$ ($\Omega_i = eB/m_i$ is the ion gyrofrequency). The electromagnetic mode propagates in the electron diamagnetic drift direction in the laboratory frame.

All of these indicate that the observed high frequency electromagnetic turbulence of 80-120 kHz in the magnetic fluctuation spectrum is MTM, which can be driven when β_e and collisionality are sufficiently high and η_e>1 in discharge #4742.

4. NONLINEAR INTERACTION AND CONFINEMENT

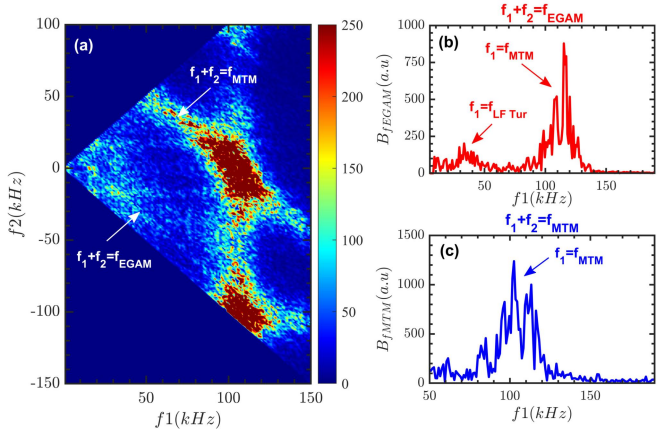

Fig. 7. Bi-spectrum of magnetic fluctuation of Mirnov signal during ECRH heating, the slice of the bi-spectrum (b) at the GAM frequency (f_1+f_2=f_{EGAM}) and (c) at the MTM frequency (f_1+f_2=f_{MTM}).

Figure 7(a) shows the bi-spectrum of magnetic fluctuations during ECRH at t=1050-1100 ms. Two oblique lines respectively corresponding to f_1+f_2=f_{EGAM} and f_1+f_2=f_{MTM} can be identified in figure 7(a) and the values of the lines are higher than the noise level. It indicates that both EGAM and MTM are interacted by the nonlinear three-wave coupling. The slice of bi-spectrum is plotted along the diagonal f_1+f_2=f_{EGAM} in figure 7(b). The highest peaks have been found around frequency f_1=f_{MTM}, corresponding to the strong nonlinear interaction between EGAM and MTM. The frequency around f_1=$f_{LF\ Tur}$ reveals the strong coupling between EGAM and low-frequency ambient turbulence (LF Tur), indicating that there is energy transfer between them. Figure 7(c) shows the slice of bi-spectrum which is plotted along the diagonal f_1+f_2=f_{MTM}. The peaks have been found around frequency f_1=f_{MTM}, indicating the strong coupling between MTM and low-frequency ambient turbulence (LF Tur).

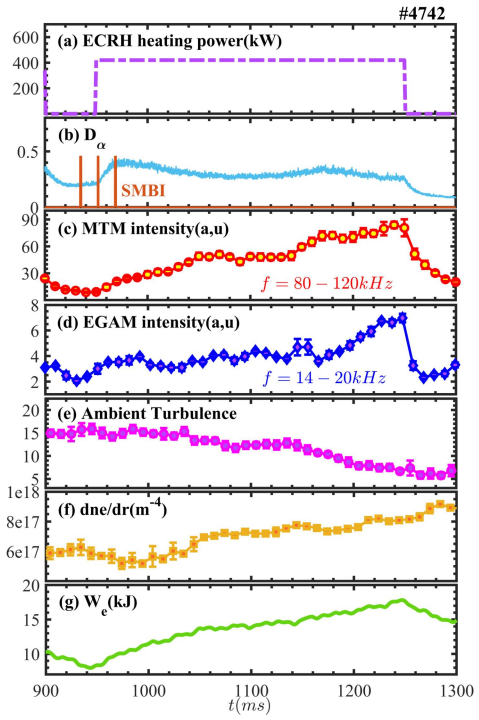

Fig. 8. (a) ECRH power, (b) D_α signal and SMBI pulses of deuterium, intensity of (c) MTM in the frequency range of 80-120 kHz, (d) EGAM in the frequency range of 14-20 kHz and (e) ambient turbulence, (f) electron density gradient around ρ=0.25 *and (g) the plasma stored energy.*

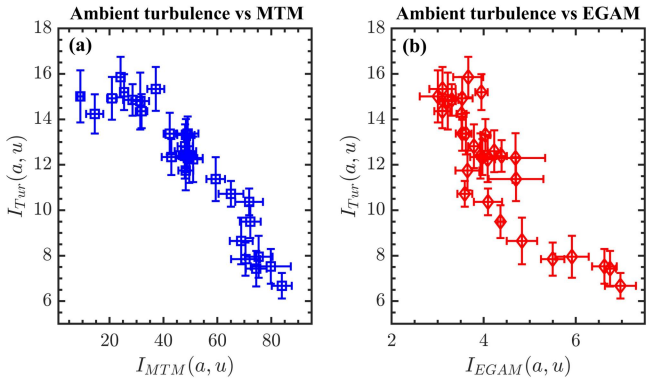

Fig. 9. Intensity of ambient turbulence that interacts with EGAM integrated over frequency range of 0-50 kHz vs intensity of MTM (a) in the frequency range of 80-120 kHz and EGAM (a) in the frequency range of 14-20 kHz at t=950-1250 ms.

As shown in figures 8 (c)(d)(e), as the increase of MTM and EGAM, the ambient turbulence decreases. The D_α signal in some cases represents the particle flux. It can be observed that the decrease in D_α indicates the reduction in particle flux as shown in figure 8(b). It can be clearly observed that the plasma stored energy and electron density gradient are increased as shown in figure 8(g) and figure 8(f), due to the reduction of ambient turbulence. Figure 9 implies that the energy transfer is in the direction of ambient turbulence to MTM and EGAM. The improvement of particle and energy confinement is resulted from MTM and EGAM reducing ambient turbulence, which suggests that the contribution from ambient turbulence on heat transport is dominant compared to MTM.

5. CONCLUSIONS AND DISCUSSIONS

In these experiments, EGAM can directly absorb and store energy from ambient turbulence. MTM can absorb energy from ambient turbulence either directly or indirectly via EGAM. The contribution from ambient turbulence on heat transport is dominant compared to MTM, the decrease of ambient turbulence results in the improvement of energy transport. These experimental results on HL-3 show that the interaction between MTM and EGAM provides a possible way to the turbulence control for energy and particle confinement improvements in fusion reactor.

ACKNOWLEDGMENTS

The authors would like to thank the HL-3 team for their supports of the experiments. The author (S.Q. Wang) sincerely thanks Prof L.W. Yan from Southwestern Institute of Physics for the valuable discussion and revision suggestions.

This work is supported by the National Key R&D Program of China under Grant Nos. 2022YFE03060001 and 2022YFE031802, and the Fundamental Research Program of CNNC under Grant No. CNNC-JCYJ-202325. It is also partially supported within the framework of the cooperation between the French Commissariat à l'Energie Atomique et aux Energies Alternatives (CEA) and the China National Nuclear Corporation (CNNC).

REFERENCES

[1] Horton W, Drift waves and transport, Rev. Mod. Phys. **71** 735 (1999).

[2] W. Guttenfelder, J. Candy, S. M. Kaye, Electromagnetic transport from microtearing mode turbulence, Phys. Rev. Lett. **106** 155004 (2011).

[3] Ehab Hassan, D.R. Hatch, M.R. Halfmoon, Identifying the Microtearing modes in the pedestal of DIII-D H-modes using Gyrokinetic simulations, Nucl. Fusion **62** 026008 (2022).

[4] M. Zuin, S. Spagnolo, I. Predebon, Experimental observation of Microtearing modes in a toroidal fusion plasma, Phys. Rev. Lett **110** 055002 (2013).

[5] D. Dickinson, C. M. Roach, S. Saarelma, Kinetic Instabilities that Limit β in the Edge of a Tokamak Plasma: A Picture of an H-Mode PedestalPhys. Rev. Lett. **108** 135002 (2012).

[6] G.D. Conway, A.I. Smolyakov, T. Ido, Geodesic Acoustic Modes in magnetic confinement devices, Nucl.Fusion **62** 013001 (2021).

[7] H.L. Berk, C.J. Boswell, D. Borba, Explanation of the JET n = 0 chirping mode, Nucl. Fusion **46** S888 (2006).

[8] G.D. Conway, C Troster, B Scott, Frequency scaling and localization of geodesic acoustic modes in ASDEX Upgrade, Plasma Phys. Control. Fusion **50** 055009 (2008).

[9] R. Nazikian, G. Y. Fu, M. E. Austin, Intense Geodesic Acousticlike Modes Driven by Suprathermal Ions in a Tokamak Plasma, Phys. Rev. Lett. **101** 185001 (2008).

[10] D. Zarzoso, X. Garbet, Y. Sarazin, Fully kinetic description of the linear excitation and nonlinear saturation of fast-ion-driven geodesic acoustic mode instability, Phys. Plasmas **19** 022102 (2012).

[11] T. Ido, Y. Miura, K. Hoshino, Observation of the interaction between the geodesic acoustic mode and ambient fluctuation in the JFT-2M tokamak, Nucl. Fusion **46** 512 (2006).

[12] D Zarzoso,Y. Sarazin, X. Garbet, Impact of Energetic-Particle-Driven Geodesic Acoustic Modes on Turbulence, Phys Rev Lett **110** 125002 (2013).

[13] X.R. Duan, M. Xu, W.L. Zhong, Progress of HL-2A experiments and HL-2M program, Nucl. Fusion **62** 042020 (2022).